

1 **Title:** Mimicking the breast metastatic microenvironment: characterization of a novel syngeneic
2 model of HER2⁺ breast cancer

3
4 **Authors:** Aaron G. Baugh¹, Edgar Gonzalez¹, Valerie H. Narumi², Jesse Kreger³, Yingtong Liu³,
5 Christine Rafie⁴, Sofi Castanon¹, Julie Jang¹, Luciane T. Kagohara^{5,6,7}, Dimitra P.
6 Anastasiadou^{8,9}, James Leatherman^{5,7}, Todd D. Armstrong^{5,6,7}, Isaac Chan¹⁰, George S.
7 Karagiannis^{8,9,11,12,13}, Elizabeth M. Jaffee^{5,6,7}, Adam MacLean³, Evanthia T. Roussos Torres¹

8
9 **Affiliations:**

10 ¹ Department of Medicine, Division of Medical Oncology, Norris Comprehensive Cancer Center,
11 Keck School of Medicine, University of Southern California, Los Angeles, CA, USA

12 ² Department of Biochemistry and Molecular Medicine, Keck School of Medicine, University of
13 Southern California, Los Angeles, CA, USA

14 ³ Department of Quantitative and Computational Biology, University of Southern California, Los
15 Angeles, CA, USA

16 ⁴ University of Miami Miller School of Medicine, Miami, FL, USA

17 ⁵ Johns Hopkins Bloomberg Kimmel Institute for Immunotherapy, Johns Hopkins University
18 School of Medicine, Baltimore, MD, USA; Cellular and Molecular Medicine, Johns Hopkins
19 University School of Medicine, Baltimore, MD, USA

20 ⁶ Johns Hopkins Convergence Institute, Johns Hopkins University School of Medicine,
21 Baltimore, MD, USA

22 ⁷ Department of Oncology, Sidney Kimmel Comprehensive Cancer Center, Johns Hopkins
23 University, Baltimore, MD, USA

24 ⁸ Department of Microbiology & Immunology, Albert Einstein College of Medicine, Bronx, NY,
25 USA

26 ⁹ Tumor Microenvironment & Metastasis Program, Montefiore-Einstein Cancer Center, Bronx,
27 NY, USA

28 ¹⁰ Department of Molecular Biology, University of Texas Southwestern Medical Center, Dallas,
29 Texas, USA

30 ¹¹ Integrated Imaging Program for Cancer Research, Albert Einstein College of Medicine, Bronx,
31 NY, USA

32 ¹² Gruss-Lipper Biophotonics Center, Albert Einstein College of Medicine, Bronx, NY, USA

33 ¹³ Cancer Dormancy and Tumor Microenvironment Institute, Albert Einstein College of Medicine,
34 Bronx, NY, USA

35

36 **Keywords:**

37 Breast cancer, cancer cell lines, cancer metastasis, mouse models, pre-clinical models,
38 syngeneic models

39

40 **Correspondence:**

41 Evanthia T. Roussos Torres

42 Phone: 310-729-0370

43 Email: Evanthia.Roussosstorres@med.usc.edu

44 Address: 1441 Eastlake Ave, Suite 6412, Los Angeles, CA, 90033

45 **ABSTRACT**

46 Preclinical murine models in which primary tumors spontaneously metastasize to distant organs
47 are valuable tools to study metastatic progression and novel cancer treatment combinations.
48 Here, we characterize a novel syngeneic murine breast tumor cell line, NT2.5-lung metastasis (-
49 LM), that provides a model of spontaneously metastatic neu-expressing breast cancer with
50 quicker onset of widespread metastases after orthotopic mammary implantation in immune-
51 competent NeuN mice. Within one week of orthotopic implantation of NT2.5-LM in NeuN mice,
52 distant metastases can be observed in the lungs. Within four weeks, metastases are also
53 observed in the bones, spleen, colon, and liver. Metastases are rapidly growing, proliferative,
54 and responsive to HER2-directed therapy. We demonstrate altered expression of markers of
55 epithelial-to-mesenchymal transition (EMT) and enrichment in EMT-regulating pathways,
56 suggestive of their enhanced metastatic potential. The new NT2.5-LM model provides more
57 rapid and spontaneous development of widespread metastases. Besides investigating
58 mechanisms of metastatic progression, this new model may be used for the rationalized
59 development of novel therapeutic interventions and assessment of therapeutic responses
60 targeting distant visceral metastases.

61 **SUMMARY STATEMENT**

62 We characterize a new syngeneic, immune-competent murine model of breast cancer (NT2.5-
63 LM) that yields rapid and widespread metastases, preserves spontaneous metastasis, and
64 provides a model for studying novel therapeutic interventions.

65 INTRODUCTION

66 Breast cancer remains one of the leading causes of cancer mortality among women worldwide,
67 with metastatic burden as the major contributor of patient death.(Riggio et al., 2020; Sung et al.,
68 2021) The development of murine models of breast cancer has provided researchers with the
69 means to more intricately study tumor initiation, progression, metastasis, and response to
70 therapies, leading to our current understanding of the complex physiological systems and
71 molecular mechanisms underlying these processes.(Kim and Baek, 2010; Park et al., 2018)
72 Various transgenic models of breast cancer that develop spontaneous mammary tumors and
73 metastases exist.(Green et al., 2000; Chantale T Guy et al., 1992; C T Guy et al., 1992; Lin et
74 al., 2004; Macleod and Jacks, 1999; Siegel et al., 2003) However, only few of these models
75 allow for efficient study of the metastatic tumor microenvironment (TME). Syngeneic models of
76 breast cancer, which involve orthotopic implantation of tumor cells or tumor chunks, are widely
77 utilized, but often times, these models are either slow-growing or do not develop clinically overt
78 metastases. Experimental metastasis models, which involve tail vein injection of tumor cells, are
79 also widely utilized, but these models are limited by lack of resolution in metastatic progression,
80 and conclusions drawn from these models may be artificial. As such, development of
81 appropriate mouse models of breast carcinoma that recapitulate metastatic progression in a
82 pathophysiological and clinically relevant context is necessary.

83 The immunotolerant MMTV-HER2/Neu (ERBB2) transgenic murine model (NeuN)
84 originally characterized by Guy et al.,(C T Guy et al., 1992) in which FVB/N strain mice express
85 the non-transforming rat *Neu* cDNA under control by a mammary tissue-specific promoter, gives
86 rise to spontaneous mammary tumors between 125 and 300 days. This model yields
87 spontaneously developing mammary tumors that closely mimic human epidermal growth factor
88 2-positive (HER2⁺) tumors.(Fry et al., 2017) One caveat of this model is its long latency for
89 development of both primary and metastatic disease, as well as the lack of penetrance of
90 metastatic disease. To circumvent these issues, previous efforts have focused on its

91 improvement and have led to the development of a syngeneic tumor cell line derivative, known
92 as NT2.5. The latter model has significantly shortened the time from tumor cell injection to tumor
93 growth and is capable of establishing widespread distant metastases upon cardiac or tail vein
94 injections.(R Todd Reilly et al., 2000; Song et al., 2008) Metastases in various organs can be
95 observed within 3 weeks of NT2.5 tumor cell injection, but this model is also limited by its
96 inability to recapitulate the process of spontaneous metastasis.

97 In this study, we report the serial passaging of the original NT2.5 cell line to generate a
98 new subline called NT2.5-LM, which represents an orthotopic, immunotolerant model of HER2⁺
99 breast cancer capable of promoting development of spontaneous metastases. We also perform
100 an in-depth characterization of the newly established NT2.5-LM cell line at both the genomic
101 and proteomic levels to establish the foundations for its potential use in preclinical studies.

102 **RESULTS**

103 **Orthotopic implantation of NT2.5-LM leads to decreased survival, larger mammary**
104 **tumors, and increased lung metastasis**

105 In the NT2.5 syngeneic model, NT2.5 cells are implanted in the mammary fat pad of adult
106 female NeuN mice, after which the maximum allowable volume of 1.5 cm³ is reached in 4-5
107 weeks,(Brian J. Christmas et al., 2018; R T Reilly et al., 2000a; Sidiropoulos et al., 2022) prior to
108 the establishment of metastatic disease and preventing efficient study of metastatic tumor
109 microenvironments (TMEs). To derive a highly metastatic cell line, lung metastases were
110 macro-dissected from the lungs of NT2.5 mammary tumor-bearing NeuN mice, dissociated to
111 single-cell suspensions, and intravenously injected into non-tumor-bearing NeuN mice, after
112 which lung metastases were harvested again and the process repeated. After the third round of
113 harvest, spontaneous lung metastases could be observed 3 weeks following mammary fat pad
114 injection of isolated cells, thus establishing the NT2.5-lung metastasis (-LM) cell line for use.

115 To characterize the phenotype of NT2.5-LM-derived tumors *in vivo*, we orthotopically
116 injected NT2.5-LM cells into the mammary fat pad of NeuN mice and measured survival, tumor
117 burden, and metastatic burden. When compared to parental NT2.5 controls, mice orthotopically
118 injected with NT2.5-LM cells experienced significantly decreased survival (**Fig. 1A**) and
119 increased weekly mammary tumor growth rates (**Fig. 1B**). Despite surgical resection of NT2.5-
120 LM mammary tumors at 12 days post-injection, tumors regrew at 24 days post-injection and
121 reached endpoint criteria faster than NT2.5 mammary tumors (**Figs. S1A-B**). Necropsy
122 analyses of mice with NT2.5-LM mammary tumors revealed widespread metastases in the
123 heart, lymph nodes, lungs, kidneys, adrenal glands, stomach, colon, spleen, skull, ears, body
124 walls, and teeth (**Fig. S2**), with high metastatic burden observed in the lungs. Moving forward,
125 we focused on the lungs as a surrogate measure of total metastatic burden. When examining
126 lungs of mice euthanized from 34 to 41 days post-injection, we found a significant increase in
127 the number of lung metastases in the NT2.5-LM model, when compared to the NT2.5 control

128 **(Fig. 1C)**. NT2.5-LM lung micro-metastases could be observed by H&E staining as early as 7
129 days post-injection, with consistent growth observed at 10, 22, 28, and 35 days post-injection
130 **(Fig. 1D)**.

131 To further illuminate on the phenotypic characteristics of NT2.5-LM metastases, we
132 performed immunohistochemical staining for ERBB2, Ki67, CK5, CK6, AE1/3, and EGFR.
133 NT2.5-LM lung metastases are ERBB2-positive **(Fig. 1E)**, express similarly low levels of AE1/3
134 and EGFR, and are similarly negative for CK5 and CK6, when compared to NT2.5 mammary
135 tumors **(Fig. S3)**. Finally, NT2.5-LM lung metastases are more proliferative, as observed by
136 increased numbers of Ki67+ cells **(Figs. 1F-G)**.

137

138 **NT2.5-LM responds to HER2 directed therapy**

139 Patients with HER2⁺ breast cancer demonstrate a response rate of over 35% when treated with
140 HER2-directed monoclonal antibody therapy.(Vogel et al., 2002) To characterize the sensitivity
141 of the NT2.5-LM model to a similar type of therapy, NT2.5-LM metastasis-bearing mice were
142 treated with anti-HER2 antibody by intraperitoneal (i.p.) injection once a week and assessed for
143 survival **(Fig. S4)**. Anti-HER2-treated mice showed improved survival when compared to
144 vehicle-treated mice, with a ~35% response rate to therapy **(Fig. 2A)**, similar to that observed in
145 patients treated with single agent therapy.(Vogel et al., 2002) When assessing the anti-HER2
146 treatment effects on lung metastases, we found that treatment did not change the number of
147 lung metastases **(Fig. 2B)**, but it significantly decreased the area of metastases within the lung
148 **(Fig. 2C)**. Together, these data suggest that the new NT2.5-LM model demonstrates clinical
149 relevance with regards to its therapeutic response to anti-HER treatments.

150

151 **NT2.5-LM does not exhibit altered mutational landscape compared to parental NT2.5**

152 With the increased number of lung metastases in NT2.5-LM model, we hypothesized that there
153 might be differences in the genomic landscape and pathogenic mutational burden between the

154 NT2.5 and NT2.5-LM tumors. First, we performed whole exome sequencing on the NT2.5 and
155 NT2.5-LM cell lines to identify potential variations in genes with known pathogenic mutations
156 and in genes known to affect proliferation and metastasis. Many pathogenic gene mutations
157 common to breast cancer (Gil Del Alcazar et al., 2022), such as *Pten*, *Brca2*, *Atm*, *Cdh1*, *Chek2*,
158 *Nf1*, *Arid1a*, *Pik3ca*, and *Esr1*, revealed no alterations between NT2.5 and NT2.5-LM (**Fig. 3A**).
159 Of note, NT2.5-LM contained mutations in *Brca1* and NT2.5 contained mutations in *Rad51c*, but
160 both were found within intron regions, thus not affecting protein sequence. Since NT2.5-LM is a
161 HER2⁺ cell line, we examined the *ErbB2* transcript sequence across both cell lines more
162 thoroughly and found six mutations within the protein coding sequence. However, all six
163 mutations were silent (**Fig. 3B**). Lastly, we assessed tumor mutational burden, given that it
164 represents another factor that could affect response to therapy. We found 11.45 mutations per
165 megabase in the NT2.5 and 13.45 mutations per megabase in the NT2.5-LM models, with
166 similar distributions of high missense mutations, single nucleotide polymorphisms (SNPs), and
167 tyrosine-to-cytosine and cytosine-to-tyrosine mutations (**Figs. 3C-D**). Collectively, these data
168 suggest that phenotypic differences between the NT2.5 and NT2.5-LM models are not the result
169 of diversified mutational burden in NT2.5-LM.

170

171 **NT2.5-LM exhibits altered signaling indicative of epithelial-to-mesenchymal transition** 172 **(EMT)**

173 Given the non-significant alterations in mutational burden, we sought to explain the differences
174 in pro-metastatic phenotypes by comparing gene expression profiles between NT2.5 and
175 NT2.5-LM. Four NT2.5 tumors and four NT2.5-LM tumors were collected from NeuN mice and
176 subjected to unsorted single-cell RNA sequencing (scRNAseq), yielding approximately 9.6×10^8
177 total reads. From Louvain clustering, approximately 10,000 NT2.5 and 9,000 NT2.5-LM cancer
178 cells were identified as *Lcn+*, *Wfd2c+*, *Cd24a+*, *Cd276+*, *Col9a1+*, *ErbB2+*, (Berger et al., 2010;
179 Gündüz et al., 2016; Seaman et al., 2017; Sidiropoulos et al., 2022; Yang et al., 2009; Yeo et

180 al., 2020) subsetted out, and visualized by Principal Component Analysis (PCA) (**Fig. 4A**). An
181 analysis of the top 25 differentially expressed genes between the two cancer cell clusters
182 revealed an upregulation of genes associated with increased cellular proliferation [*Pdgfa*,
183 *Sox9*],(Jansson et al., 2018; Ma et al., 2020; Pinto et al., 2014) invasion and migration [*Lrp1*,
184 *Cd9*, *Cxcl1*, *Anxa1*],(Fayard et al., 2009; Moraes et al., 2018; Rappa et al., 2015; Xing et al.,
185 2016; Yang et al., 2019) epithelial-to-mesenchymal transition (EMT) [*Vim*, *Inhba*], (Paulin et al.,
186 2022; Yu et al., 2021) and stemness and metastatic potential [*S100A4*, *Nrp2*, *Aldh2*,
187 *JunB*](Elaimy et al., 2018; Helfman et al., 2005; Qiao et al., 2015; Sundqvist et al., 2018;
188 Yasuoka et al., 2009; Zhang and Fu, 2021) in NT2.5-LM. Concurrently, there was a
189 downregulation of genes associated with decreased cellular proliferation [*Crip1*],(Ludyga et al.,
190 2013) decreased invasion [*Cldn7*],(Kominsky et al., 2003; Martin and Jiang, 2009) and
191 decreased epithelial phenotype and polarization [*Epcam*](Kyung-A Hyun et al., 2016) in NT2.5-
192 LM (**Figs. 4B-C**). We validated the increased gene expression of *Vim* and decreased gene
193 expression of *Epcam* in NT2.5-LM at the protein level by flow cytometry, demonstrating a
194 significant increase in the percentage of Vimentin-positive cells and significant decrease in the
195 percentage of Epcam-positive cells. (**Figs. 4D-E**).

196 Further investigation into differential pathway regulation was performed by comparing
197 the top 250 differentially expressed genes for overlap with pathways from the
198 'KEGG_2019_Mouse' database using Gene Set Enrichment Analysis. NT2.5-LM exhibited
199 significant upregulation of the glycolysis pathway and downregulation of oxidative
200 phosphorylation, ECM-receptor interaction, focal adhesion, protein digestion and absorption,
201 and adherens junction pathways ($p\text{-adj} < 0.05$) (**Fig. S5, Table S1**). Dissolution of adherens
202 junctions and alterations in cell-cell interactions is a hallmark of EMT,(Kalluri and Weinberg,
203 2009; Liu et al., 2016) and these data offer increased EMT as an explanation for the increased
204 metastatic phenotype of NT2.5-LM.

205

206 **NT2.5-LM expresses increased levels of Mena^{INV} – a marker of metastatic potential**

207 Our group has performed extensive work on mechanisms of metastatic dissemination and has
208 previously reported that pro-migratory/pro-invasive tumor cells primed for the metastatic journey
209 tend to upregulate the expression of Mena^{INV}, a spliced isoform of the actin-regulatory protein
210 mammalian enabled (Mena) that conveys increased metastatic potential. Specifically, previous
211 studies have collectively shown that Mena^{INV} is correlated with increased breast cancer cell
212 migration, invasion, and metastasis, (Borriello et al., 2022; Karagiannis et al., 2016; Philippar et
213 al., 2008; Roussos et al., 2011b; Sharma et al., 2021) and is significantly upregulated in
214 response to cytotoxic treatments. (Karagiannis et al., 2017) In view of observed alterations in
215 various ECM and cell-cell adhesion interaction pathways, (**Fig. S5, Table S1**), we expected an
216 enrichment of Mena^{INV}-positive tumor cells in NT2.5-LM metastatic tumors. Indeed,
217 immunofluorescence analysis of Mena^{INV} revealed significantly increased expression in the
218 metastatic NT2.5-LM tumors, when compared to the NT2.5 mammary tumors (**Figs. 5A-B**).

219 **DISCUSSION**

220 Spontaneously metastatic breast cancer cell lines are valuable tools for studying how metastatic
221 tumors differ from primary tissue tumors in mice, but the time for spontaneous lung metastases
222 to develop after injection of cancer cells into the breast tissue site is prolonged and inconsistent.
223 In this study, we generated a more aggressively metastatic breast cancer cell line, NT2.5-LM,
224 that spontaneously metastasizes to distant organs as early as one week post-injection. This not
225 only allows us to study the effects of treatment interventions on metastatic progression in the
226 most biologically accurate setting, but also utilizes surgical removal of the primary tumor early
227 on to ensure that we are not limited by humane endpoints of primary tumor growth.

228 NT2.5-LM exhibited poorer survival, faster primary tumor growth, and more widespread
229 metastases. Because the NT2.5-LM cell line was derived from NT2.5, we sought to understand
230 the differences that would cause it to be more widely metastatic and proliferative compared to
231 the parental cell line. We hypothesized that increased expression of HER2 or a novel mutation
232 in the *ErbB2* gene could be driving increased proliferation. NT2.5-LM did not exhibit new
233 pathogenic mutations in *ErbB2*, and increased expression of HER2 was not observed by
234 immunohistochemistry. Furthermore, pathways analyses conducted on scRNAseq data
235 demonstrated no significant difference in expression of genes within the ErbB pathway. Thus,
236 change in HER2 signaling is not a likely mechanism driving the increased metastatic and
237 proliferative phenotype observed in NT2.5-LM.

238 Other potential mechanisms driving observed differences in NT2.5-LM include the
239 differential regulation of proliferation- and metastasis-promoting pathways. We observed a shift
240 in metabolic pathways with an upregulation of glycolysis and a downregulation of oxidative
241 phosphorylation KEGG pathways, which have been previously implicated in more metastatic
242 cancers,(Ashton et al., 2018; Gaude and Frezza, 2016) supporting our observations that NT2.5-
243 LM is more widely metastatic. We observed a downregulation of ECM receptor interaction, focal
244 junction, and adheres junction pathways, which are interactors in the intravasation and

245 extravasation processes of metastasis.(Fares et al., 2020) We also identified differential
246 expression of key genes involved in EMT that favored a more mesenchymal phenotype in
247 NT2.5-LM, which could explain the increased number of metastases in lung and other distant
248 organs. Our observed alterations in expression of epithelial markers, mesenchymal markers,
249 cell adhesion pathways, extracellular matrix pathways, and metabolic pathways are
250 characteristic of EMT.(Le Bras et al., 2012; Pal et al., 2022)

251 One interesting alteration associated with the loss of epithelial cell-cell contacts is the
252 increased expression of invasive actin regulatory protein isoform Mena^{INV}.(Goswami et al.,
253 2009) Mena^{INV}-expressing breast cancer cells participate in a paracrine loop with intratumoral
254 macrophages, which facilitates their translocation to the perivascular niche. Once they reach the
255 vasculature, Mena^{INV}-expressing tumor cells associate with perivascular macrophages to
256 intravasate into the blood vessel. These tripartite microanatomical structures composed of
257 endothelial cells, perivascular macrophages, and Mena^{INV}-expressing tumor cells are key
258 prerequisites of metastatic dissemination and have been previously called Tumor
259 Microenvironment of Metastasis (TMEM) doorways.(Borriello et al., 2022; Karagiannis et al.,
260 2017; Philippar et al., 2008; Robinson et al., 2009; Roussos et al., 2011a; Sharma et al., 2021)
261 Of note, NT2.5-LM tumors exhibit increased expression of Mena^{INV}, which could explain its
262 highly metastatic nature. As such, this model may be efficiently used in the future to study
263 mechanisms of breast cancer cell dissemination associated with TMEM doorways and Mena^{INV}-
264 dependent pathways.

265 In summary, our findings distinguish NT2.5-LM as a more proliferative and metastatic
266 model of breast cancer for experimental use that also preserves the spontaneous metastatic
267 process within a shorter timeline. Various genetic and epigenetic changes can occur in a cancer
268 cell as it accumulates mutations, proceeds through EMT, interacts with the TME, and forms
269 distant metastases. Our group and others have shown that the addition of epigenetic
270 modulators to various therapies in multiple cancer models has decreased tumor growth and

271 improved response.(Brian J. Christmas et al., 2018; Kim et al., 2014; Orillion et al., 2017;
272 Sidiropoulos et al., 2022) Moving forward, we envision the use of this NT2.5-LM model to
273 facilitate efficient future studies of novel treatment combinations for metastatic disease and
274 evaluation of different metastatic TME contributions to therapeutic response.

275 **METHODS**

276 **Cell lines**

277 NT2.5-lung metastasis (-LM) cell line was derived from the parental NT2.5 cell line, which was
278 originally derived from the NT2 cell line in the NeuN murine model established by Guy et al.(C T
279 Guy et al., 1992) 1×10^5 NT2.5 cells were injected intravenously by tail vein in five 8-week-old
280 female NeuN mice. Three weeks after tail vein injection, lung metastases were macro-dissected
281 from all mice, minced on ice, filtered using a 100 μm filter, and pooled. The pooled cells were
282 used to repeat the process described above, starting with intravenous injection, and after the
283 third round of lung metastasis harvest, pooled cells were injected into the mammary fat pad of
284 five 8-week-old female NeuN mice for spontaneous lung metastasis formation. After
285 confirmation of spontaneous lung metastasis formation by lung harvest and Hematoxylin and
286 Eosin (H&E) stains, the cell line was propagated in cell culture and named NT2.5-LM. NT2.5
287 cells were derived from spontaneous mammary tumors growing in female NeuN mice and
288 obtained from the Jaffee Lab at Johns Hopkins University.(Jaffee et al., 1998; Machiels et al.,
289 2001; R T Reilly et al., 2000b) Culture conditions for NT2.5-LM and NT2.5 cells are as follows:
290 37°C, 5% CO₂ in RPMI 1640 (Gibco, cat. 11875-093) supplemented with 20% fetal bovine
291 serum (Gemini, cat. 100-106), 1.2% HEPES (Gibco, cat. 15630-080), 1% L-glutamine (Gibco,
292 cat. 25030-081), 1% MEM non-essential amino acids (Gibco, cat. 11140-050), 0.5%
293 penicillin/streptomycin (Gibco, cat. 15140-122), 1% sodium pyruvate (Sigma, cat. S8636), 0.2%
294 insulin (NovoLog, cat. U-100). Cell lines are tested for mycoplasma every 6 months.

295

296 **Mice**

297 A syngeneic mouse model of HER2⁺ breast cancer using the NT2.5 cell line was derived from
298 the NeuN transgenic mouse developed by Guy et al.(C T Guy et al., 1992) NeuN transgenic
299 mice overexpress non-transforming rat neu cDNA under the control of a mammary specific
300 promoter and develop spontaneous focal mammary adenocarcinomas after a long latency of

301 125 days with the majority of mice developing tumors by 300 days. Injection of NT2.5 into NeuN
302 mice leads to development of tumors 100% of the time, since these mice are tolerized to Neu.
303 Mice were kept in pathogen-free conditions and were treated in accordance with institutional
304 and American Association of Laboratory Animal Committee policies. NeuN mice were originally
305 from W. Muller McMaster University, Hamilton, Ontario, Canada and overexpress HER2 via the
306 mouse mammary tumor virus (MMTV) promoter. Colonies are renewed yearly from Jackson
307 labs and bred in-house by brother/sister mating.

308

309 **Survival, tumor growth, metastasis growth, necropsy**

310 1×10^5 NT2.5 or NT2.5-LM cells were injected into the mammary fat pad. NT2.5-LM tumors were
311 resected on day 12. Survival endpoint was determined to be mammary tumor volume exceeding
312 1.5 cm^3 or morbidity symptoms due to lung metastatic tumor burden, such as breathing, coat
313 condition, activity, and posture. Mammary tumor growth was measured by calipers ($\pm 0.01 \text{ mm}$)
314 three times a week, with weekly tumor growth determined by calculating the average of
315 differences in tumor volumes per week for each mouse. Lung surface metastases were counted
316 by visual inspection of collected lungs following euthanasia at survival endpoint and before
317 fixation in formalin and paraffin-embedding. Lung sections were taken $40 \mu\text{m}$ apart, for a
318 representative 3 sections per lung. H&E stained sections were scanned and analyzed using
319 either HALO or NDPView.2 to quantify number and tumor area of lung metastases. For
320 necropsy, various tissues were collected at survival endpoint, fixed in formalin, paraffin-
321 embedded, sectioned, stained with H&E, and visualized by light microscopy. Necropsy tissues
322 include heart, lymph nodes, lungs, kidney, adrenal gland, stomach, colon, spleen, skull, ear,
323 body wall, and teeth.

324

325 **Immunohistochemistry**

326 Immunohistochemistry staining was performed at the Oncology Tissue Services Core of Johns
327 Hopkins University. Immunolabeling for ErbB2, Ki67, CK5, CK6, AE1/3 and EGFR was
328 performed on formalin-fixed, paraffin-embedded sections. Briefly, following dewaxing and
329 rehydration, slides were immersed in 1% Tween-20, then heat-induced antigen retrieval was
330 performed in a steamer using Antigen Unmasking Solution (catalog# H-3300, Vector Labs) for
331 25 minutes. Slides were rinsed in PBST, endogenous peroxidase and phosphatase were
332 blocked (Dako, cat. S2003), and then incubated with the following primary antibodies for 45
333 minutes at room temperature: anti-ErbB2 (1:400 dilution; ThermoFisher Scientific, cat. MA5-
334 15050, SF23975824), anti-Ki67 (1:200 dilution; Abcam, cat. Ab16667), anti-EGFR (1:50 dilution;
335 LSBio, cat. LS-B2914-50), anti-CK5 (1:2000 dilution; BioLegend, cat. 905501), anti-CK6 (1:200
336 dilution; Novus Biologicals, cat. NBP2-34358), anti-AE-1/AE-3 (1:200 dilution; Novus
337 Biologicals, cat. NBP2-29429). Slides were then incubated with HRP-conjugated anti-rabbit
338 secondary antibody (Leica Microsystems, cat. PB6119) for 30 minutes at room temperature.
339 Signal detection was conducted with 3,3'-Diaminobenzidine (Sigma-Aldrich, cat. D4293).
340 Counterstaining was conducted with Mayer's hematoxylin.

341

342 **Anti-HER2 treatment of mice**

343 1×10^5 NT2.5-LM cells were injected into the mammary fat pad. Mammary tumors were resected
344 on day 12, after which mice were treated with anti-HER2 antibody starting on day 23 to mimic
345 standard therapy treatment with trastuzumab in patients with HER2⁺ breast cancer. Anti-HER2
346 monoclonal antibody (BioXCell, clone 7.16.4) and mouse IgG2a isotype vehicle antibody
347 (BioXCell, clone C1.18.4) were administered at 100 μ g/mouse by intraperitoneal (i.p.) injection
348 once a week for three weeks as described.(Brian J Christmas et al., 2018) Following three
349 weeks of treatment, either lung tissues were collected for tumor burden analysis, or
350 maintenance dosing was continued once a week until survival endpoint. For tumor burden
351 analysis, three different levels were taken from formalin-fixed and paraffin-embedded lungs

352 sectioned 100 μm apart. Slides were H&E stained, scanned, and analyzed using HALO to
353 obtain summed lung metastasis counts and percent tumor area.

354

355 **Tumor dissociation**

356 Following collection, mammary tumors were minced on ice and dissociated using a tumor
357 dissociation kit (Miltenyi Biotec, cat. 130-096-730) and the 37C_m_TDK_2 program on the
358 OctoDissociator (Miltenyi Biotec) per the manufacturer's instructions. Cell suspensions were
359 filtered using 70 μm cell strainers and red blood cells were lysed using ACK lysis buffer (Quality
360 Biological, cat. 118-156-721). To submit for RNA sequencing, dead cells were removed using
361 the MACS Dead Cell Removal Kit (Miltenyi Biotec).

362

363 **Flow cytometry**

364 NT2.5 and NT2.5-LM cells were cultured for at least two passages, washed with PBS, and
365 stained with Live/Dead Fixable Aqua (ThermoFisher, cat. L10119) for 30 minutes at 4°C, per the
366 manufacturer's instructions. Cells were fixed and permeabilized for 30 minutes at room
367 temperature using the Foxp3 / Transcription Factor Staining Buffer Set (Life Technologies
368 Corp., cat. 00-5523-00), followed by an Fc receptor block (BD Pharmingen, cat. 553142) for 10
369 minutes at room temperature. Cells were incubated with the following primary antibodies for 30
370 minutes at room temperature: anti-Vimentin (1:100 dilution; Cell Signaling Technology, cat.
371 5741), anti-Epcam (1:100 dilution; Cell Signaling Technology, cat. 93790). Cells were then
372 incubated with FITC-conjugated anti-rabbit secondary antibody (1 $\mu\text{g}/\text{mL}$; BioLegend, cat.
373 406403) for 30 minutes at room temperature. Samples were run on the Attune NxT flow
374 cytometer (Invitrogen) and analyzed using Kaluza software.

375

376 **Mena^{INV} Immunofluorescence and Image Analysis**

377 Immunofluorescence staining for Mena^{INV} was performed on formalin-fixed, paraffin-embedded
378 (FFPE) sections. Briefly, slides were deparaffinized by melting for 5 minutes at 58°C in an oven
379 equipped with a fan, followed by two Xylene treatments for 20 minutes each. Slides were
380 rehydrated and antigen retrieval was performed in 1 mM EDTA, pH 8.0 for 20 minutes at 97°C
381 in a conventional steamer. Slides were washed with 0.05% PBST and incubated in blocking
382 solution (5% goat serum in 0.05% PBST) for 1 hour at room temperature. Slides were then
383 incubated with anti-Mena^{INV} primary antibody (0.25 ug/mL; in-house developed in the lab of Dr.
384 John S. Condeelis, AE1071, AP-4) overnight at 4°C. After three washes in 0.05% PBST, slides
385 were incubated with Alexa 488-conjugated goat anti-chicken secondary antibody at room
386 temperature for 1 hour. After three washes in 0.05% PBST, slides were incubated with spectral
387 DAPI for 5 minutes and mounted with ProLong Gold Antifade Mountant (Life Technologies, cat.
388 P36930). Slides were imaged using the Panoramic 250 Flash II digital whole slide scanner. Up
389 to 10 High-Power Field (HPF) images per mouse, depending on tumor and metastasis burden
390 availability, were captured in TIFF format using Caseviewer v2.4 (3DHISTECH). Further image
391 processing was performed in ImageJ. Single Mena^{INV} channels were uploaded, converted to 8-
392 bit, and binarized using intensity thresholding (default method). The DAPI channel confirmed
393 that all HPFs chosen were within necrosis-free areas of the tumors and metastases. The
394 Mena^{INV+} area in each HPF was then expressed as a fraction of the total tumor area, and the
395 mean of all HPFs was calculated for each mouse. For visualization purposes only, images were
396 enhanced in Caseviewer by exclusively using linear image modifications (i.e., brightness and
397 contrast), and the signal was pseudo-colored for optimal representation of fields of interest.

398

399 **Whole exome sequencing (WES)**

400 NT2.5 and NT2.5-LM cell lines were cultured as described above and sent for whole exome
401 sequencing at the Johns Hopkins Genomics Core. One microgram or more of mouse genomic
402 DNA from each sample was analyzed by whole exome sequencing using the SureSelectXT

403 Mouse All Exon kit (Agilent), followed by next generation sequencing using the NovaSeq 6000
404 S4 flow cell (Illumina) with a 2x150bp paired-end read configuration, per the manufacturer's
405 instructions. bcl2fastq v2.15.0 (Illumina) was used to convert BCL files to FASTQ files using
406 default parameters. Running alignments against the mm10 genome was done by bwa v0.7.7
407 (mem) along with Piccard-tools1.119 to add read groups and remove duplicate reads. GATK
408 v3.6.0 base call recalibration steps were used to create a final alignment file. MuTect2 v3.6.0
409 was used to call somatic variants against a panel of normal using default parameters. snpEFF
410 (v4.1) was used to annotate the variant calls and to create a clean tab separated table of
411 variants. IGV v2.13.2 was used to identify breast cancer specific mutations from MuTect2 files.
412 SnapGene Viewer v.6.2 was used to visually align and determine the mutations between the
413 two cell lines against the mRNA sequences of selected genes. Annotations were created to
414 visualize mutational differences.

415

416 **Single cell RNA sequencing (scRNA-seq)**

417 For library preparation, 10x Genomics Chromium Single Cell 3' RNA-seq kits v3 were used.
418 Gene expression libraries were prepared per the manufacturer's instructions. 4 biological
419 replicates totaling 8 processed tumors were sequenced in 2 batches: Run A - 2 NT2.5 tumors, 2
420 NT2.5-LM tumors; Run B - 2 NT2.5 tumors, 2 NT2.5-LM tumors. These tumors were taken as a
421 subset from a larger batch of tumors that include various mouse treatments, with each batch
422 having an equal assortment of samples from multiple treatment groups to reduce technical
423 biases. Here, we restrict our analysis to replicates under the vehicle treatment condition.
424 Illumina HiSeqX Ten or NovaSeq were used to generate total reads. Paired-end reads were
425 processed using CellRanger v3.0.2 and mapped to the mm10 transcriptome with default
426 settings. ScanPy v1.8.2 and Python v3 was used for quality control and basic filtering.
427 DoubleDetection v4.2 with Louvain clustering algorithm v0.7.1 was used to find doublets. For
428 gene filtering, all genes expressed in less than 3 cells within a tumor (NT2.5 and NT2.5-LM)

429 were removed. Cells expressing less than 200 genes or more than 8,000 genes or having more
430 than 15% mitochondrial gene expression were also removed. Gene expression was total-count
431 normalized to 10,000 reads per cell and log transformed. Highly variable genes were identified
432 using default ScanPy parameters, and the total counts per cell and the percent mitochondrial
433 genes expressed were regressed out. Finally, gene expression was scaled to unit variance and
434 values exceeding 10 standard deviations were removed. Neighborhood graphs were
435 constructed using 10 nearest neighbors and 30 principal components. Tumors were clustered
436 together within cell lines using Louvain clustering (with resolution parameter 0.12) and cancer
437 cells were identified as *Lcn+*, *Wfd2c+*, *Cd24a+*, *Cd276+*, *Col9a1+*, *ErbB2+*. (Berger et al., 2010;
438 Gündüz et al., 2016; Seaman et al., 2017; Sidiropoulos et al., 2022; Yang et al., 2009; Yeo et
439 al., 2020) All other cell clusters and doublets were removed. There were ~10,000 NT2.5 cancer
440 cells and ~9,000 NT2.5-LM cancer cells, and these were combined by total raw count
441 normalization to 10,000 reads, with log transformation and batch correction on cell lines via
442 ComBat. The 250 top differentially expressed genes in the cancer clusters from each cell line
443 were identified using the Wilcoxon rank-sum test and compared for overlap with pathways from
444 the 'KEGG_2019_Mouse' database using GSEAPY (Gene Set Enrichment Analysis in Python).
445

446 **Statistics**

447 For survival curves, Mantel-Cox log rank tests were used. For tumor growth rate, metastasis
448 counts, and lung metastasis volumes, Mann Whitney tests were used. For quantification of
449 immunohistochemistry staining, Welch's T-tests were used. For flow cytometry, unpaired t-tests
450 were used. For immunofluorescence staining of tumor and metastatic tissues, Mann Whitney U-
451 tests were used. To aid in statistical choice, data were tested for normality using D'Agostino-
452 Pearson omnibus normality tests, Anderson-Darling tests, Shapiro-Wilk normality tests, and
453 Kolmogorov-Smirnov normality tests.

454

455

456 **DECLARATIONS**

457 *Acknowledgements:* We would like to thank all members of the Elizabeth Jaffee and Elana
458 Fertig lab for help throughout the course of these experiments. Additionally, we would like to
459 thank the Molecular Genomics Core at USC, the Flow Cytometry Core at USC, the Translational
460 Pathology Adult Tissue Core at USC, the SKCCC Experimental and Computational Genomics
461 Core at Johns Hopkins, and the Oncology Tissue Services Core at Johns Hopkins for help with
462 sequencing experiments, specimen processing, and data processing. We would like to thank
463 the Analytical Imaging Facility at the Albert Einstein College of Medicine for
464 immunofluorescence and tissue slide scanning. We would also like to acknowledge Srinivasan
465 Yegnasubramanian and Emma Bigelow from the Johns Hopkins research group for data review.

466

467 *Funding:* This work was supported through funding from: Tower Cancer Research Foundation
468 Career Development Award (ETRT); P30CA014089 from the National Cancer Institute (ETRT);
469 NIH NCI P30 CA014089 (ETRT); MacMillan Pathway to Independence Fellowship (ETRT);
470 Concern Foundation Conquer Cancer Now Award (ETRT); USC NCCC Core Voucher Program,
471 NIH (NCI R01CA184926 for EMJ; P50CA062924 for EMJ, and LTK; NCI R01CA177669 for
472 LTK); the Broccoli Foundation (EMJ and ETRT); The Bloomberg-Kimmel Institute for Cancer
473 Immunotherapy; The Skip Viragh Center for Pancreas Cancer Clinical Research and Patient
474 Care; The Commonwealth Foundation for Cancer Research (SY, ETRT, LTK); the Allegheny
475 Foundation (LTK); the Emerson Foundation (EMJ); the Maryland Cigarette Restitution Fund
476 (SY); Cancer Center Support Grant (P30CA013330 for GSK); Share Instrumentation Grant
477 (1S10OD026852-01A1 for GSK); NIH-NCI K99/R00 Transition to Independence Award
478 (R00CA237851 for GSK); the Integrated Imaging Program for Cancer Research IIPCR (GSK);
479 the Evelyn-Lipper Charitable Foundation (GSK); the Montefiore-Einstein Comprehensive
480 Cancer Center (MECC) start-up fund (GSK).

481

482 Availability of data and materials: All WES and scRNAseq raw and processed data files will be
483 made available on NCBI BioProject.

484

485 Competing interests: EMJ is a paid consultant for Adaptive Biotech, CSTONE, Achilles,
486 DragonFly, and Genocea. She receives funding from Lustgarten Foundation and Bristol Myer
487 Squibb. She is the Chief Medical Advisor for Lustgarten and SAB advisor to the Parker Institute
488 for Cancer Immunotherapy (PICI) and for the C3 Cancer Institute.

489

490 Ethics approval and consent to participate: All animal studies were approved by the Institutional
491 Review Board of USC and Johns Hopkins University.

492 **FIGURE LEGENDS**

493 **Figure 1: NT2.5-LM leads to decreased survival, larger mammary tumors, and increased**
494 **lung metastasis. (A)** 1×10^5 NT2.5 or NT2.5-LM cells were injected into the mammary fat pad of
495 NeuN mice (NT2.5, n=10; NT2.5-LM, n=7). After surgical resection of NT2.5-LM tumor-bearing
496 mice at 12 days post-injection (dpi), mice were allowed to reach humane survival endpoint with
497 tumor volume exceeding 1.5 cm^3 . **(B)** Mammary tumor sizes of mice in (A) were measured at
498 least 3x a week by calipers, averaged, and used to calculate differences in average weekly
499 tumor growth rate. **(C)** At survival endpoint of mice in (A), the number of surface metastases
500 was counted by visual inspection. **(D)** H&E staining of lungs in NT2.5-LM tumor-bearing mice
501 collected at 7, 10, 22, 28, and 35 days post-injection (dpi). Black arrows point to lung
502 metastases. Scale bars as shown. **(E)** Immunohistochemistry (IHC) staining of Erbb2 and **(F)**
503 Ki67 in NT2.5 mammary tumors (top) and NT2.5-LM lung metastases (bottom) collected at 35
504 days post-injection. Scale bars as shown. **(G)** Percentage of Ki67+ cells from 10 regions of
505 interest (ROIs) were counted from Ki67 IHC staining in (F). Statistics used: Mantel-Cox Log-
506 rank test for (A), Mann-Whitney U-test for (B-D), Welch's T-test for (G), * $p < 0.05$, ** $p < 0.01$,
507 **** $p < 0.0001$.

508
509 **Figure 2: NT2.5-LM responds to HER2-directed therapy. (A)** 1×10^5 NT2.5-LM cells were
510 injected into the mammary fat pad of NeuN mice. After surgical resection of NT2.5-LM tumor-
511 bearing mice at 12 days post-injection (dpi), treatment with vehicle or anti-HER2 monoclonal
512 antibody (100 $\mu\text{g}/\text{mouse}$, 1x/week, intraperitoneal injection) began at 23 dpi (n=12 per treatment
513 group) and continued until survival endpoint at 70 dpi. **(B)** 1×10^5 NT2.5-LM cells were injected
514 into the mammary fat pad of NeuN mice, tumors were surgically resected at 12 dpi, and anti-
515 HER2 treatment (100 $\mu\text{g}/\text{mouse}$, 1x/week, intraperitoneal injection) began at 23 dpi (n=10 per
516 treatment group). Lungs were collected at 38 dpi. Three different levels were taken from
517 formalin-fixed and paraffin-embedded lungs sectioned 100 μm apart. Slides were H&E stained,

518 scanned, and analyzed using HALO to obtain summed lung metastasis counts and **(C)** percent
519 tumor area over normal lung tissue. Two mice in the vehicle group were removed due to
520 inconsistencies between HALO results and physical examination of H&E slides. Statistics used:
521 Mantel-Cox Log-rank test for (A), Mann-Whitney U-test for (B-C), ns = not-significant, **p < 0.01.

522

523 **Figure 3: NT2.5-LM does not exhibit altered mutational landscape compared to parental**

524 **NT2.5. (A)** Alignment of NT2.5 and NT2.5-LM whole exome sequencing reads to the mm10

525 genome reveal cell line-specific and –overlapping mutations common in breast cancer. **(B)**

526 *ErbB2* transcript sequence with identified mutation sites in NT2.5 and NT2.5-LM. All mutations

527 were identified to be silent mutations. Nucleotide numbering is based on DNA reference

528 sequence NM_001003817.1. Note that the version number of this reference sequence may be

529 frequently updated. **(C)** Distributions of mutation classifications, variant types, single nucleotide

530 variant (SNV) classes, and top 10 mutated genes for NT2.5 and **(D)** NT2.5-LM are shown.

531

532 **Figure 4: NT2.5-LM exhibits altered signaling indicative of increased EMT. (A)** Four NT2.5

533 and four NT2.5-LM mammary tumors were collected from NeuN mice, dissociated to single cell

534 suspensions, and sent for unsorted single-cell RNA sequencing. Cancer cell clusters were

535 annotated as *Lcn+*, *Wfd2c+*, *Cd24a+*, *Cd276+*, *Col9a1+*, *ErbB2+*, and subsetted out for PCA

536 visualization. **(B)** Top 25 significantly up- and down-regulated genes in NT2.5-LM. **(C)** Violin

537 plots of key metastasis-related genes identified in (B). **(D)** Flow cytometry staining of epithelial-

538 to-mesenchymal transition (EMT) related genes identified in (C) in NT2.5 and NT2.5-LM cell

539 lines for Vimentin and **(E)** *Epcam*. Statistics used: Unpaired T-test for (D-E), ****p < 0.0001.

540

541 **Figure 5: NT2.5-LM expresses increased levels of Mena^{INV} – a marker of metastatic**

542 **potential. (A)** Representative immunofluorescence images of Mena^{INV} (red) and DAPI (blue)

543 staining in NT2.5 mammary tumor (top), and NT2.5-LM lung metastases (bottom) collected 34-

544 41 days post-injection (dpi). Middle column and right column panels correspond to dotted
545 square in left column panels. Scale bars as shown. **(B)** Quantification of Mena^{INV} staining from
546 NT2.5 mammary tumor (n=6) and NT2.5-LM lung metastases (n=6) by averaging signal
547 intensity from up to 10 regions of interest (ROIs) in each sample. Statistics used: Mann-Whitney
548 U-test for (B), **p < 0.01.

549
550 **Figure S1: Tumor growth in NT2.5-LM model.** **(A)** 1×10^5 NT2.5 or NT2.5-LM cells were
551 injected into the mammary fat pad of NeuN mice (NT2.5, n=10; NT2.5-LM, n=7). Mammary
552 tumor volumes (mm^3) were averaged across all mice within the same group. Surgical resection
553 of NT2.5-LM tumor-bearing mice at 12 days post-injection (dpi) is depicted by a red arrow.
554 Mammary tumors regrew in NT2.5-LM at 24 dpi. Data shown until first mouse death recorded at
555 33 dpi. **(B)** Mammary tumor volumes (mm^3) of individual mice shown in (A) until required
556 euthanasia of mice.

557
558 **Figure S2: Necropsy of NT2.5-LM metastases-bearing tissues.** Upon euthanasia of NT2.5-
559 LM mice, various tissues were collected, fixed, sectioned, stained with H&E, and evaluated for
560 the presence of metastases. Tissues shown include (A) heart [scale bars: 1000 μm], (B) lymph
561 nodes [scale bars: 50 μm , 1000 μm], (C) lungs [scale bar: 2500 μm], (D) kidney [scale bar: 500
562 μm], (E) adrenal gland [scale bar: 500 μm], (F) stomach [scale bars: 500 μm , 1000 μm], (G)
563 colon [scale bars: 400 μm , 2500 μm], (H) spleen [scale bar: 250 μm], (I) skull [scale bar: 2500
564 μm], (J) ear [scale bar: 5000 μm], (K) body wall [scale bar: 2500 μm], and (L) teeth [scale bars:
565 50 μm , 750 μm].

566
567 **Figure S3: Immunohistochemistry (IHC) of NT2.5 mammary tumors and NT2.5-LM lung**
568 **metastases.** Staining of EGFR, AE1/3, CK5, and CK6 in NT2.5 mammary tumors (left) and

569 NT2.5-LM lung metastases (right) collected at 35 days post-injection. Scale bars are 280 μm
570 and 60 μm (zoomed-in panels).

571

572 **Figure S4: Anti-HER2 treatment scheme for NT2.5-LM.** 1×10^5 NT2.5-LM cells were
573 orthotopically injected in the mammary fat pad. Mammary tumors were surgically resected 12
574 days post-injection (dpi). Anti-HER2 monoclonal antibody treatment of 100 $\mu\text{g}/\text{mouse}$
575 administered intraperitoneally once a week for three weeks began at 23 dpi. After three weeks
576 of anti-HER2 treatment, maintenance dosage for survival experiments were given once a week.
577 For metastatic burden analysis, lungs were collected at 38 dpi for subsequent analysis.

578

579 **Figure S5: Differential pathway regulation in NT2.5-LM compared to NT2.5 cancer cells.**
580 Unsupervised pathways analysis from single cell RNA sequencing datasets by comparing top
581 250 differentially expressed genes with overlap in pathways from 'KEGG_2019_Mouse'
582 database using Gene Set Enrichment Analysis. Top 20 pathways in NT2.5-LM that are **(A)**
583 down-regulated and **(B)** up-regulated compared to NT2.5 are shown.

584

585 **Table S1: Differential pathways in NT2.5-LM compared to NT2.5 cancer cells.** All
586 unsupervised pathways analysis from single cell RNA sequencing datasets by comparing top
587 250 differentially expressed genes with overlap in pathways from 'KEGG_2019_Mouse'
588 database using Gene Set Enrichment Analysis.

589

590

591

REFERENCES

- Ashton, T.M., Gillies McKenna, W., Kunz-Schughart, L.A., Higgins, G.S., 2018. Oxidative phosphorylation as an emerging target in cancer therapy. *Clinical Cancer Research* 24, 2482–2490. <https://doi.org/10.1158/1078-0432.CCR-17-3070/274584/AM/OXIDATIVE-PHOSPHORYLATION-AS-AN-EMERGING-TARGET-IN>
- Berger, T., Cheung, C.C., Elia, A.J., Mak, T.W., 2010. Disruption of the *Lcn2* gene in mice suppresses primary mammary tumor formation but does not decrease lung metastasis. *Proc Natl Acad Sci U S A* 107, 2995–3000. https://doi.org/10.1073/PNAS.1000101107/SUPPL_FILE/PNAS.201000101SI.PDF
- Borriello, L., Coste, A., Traub, B., Sharma, V.P., Karagiannis, G.S., Lin, Y., Wang, Y., Ye, X., Duran, C.L., Chen, X., Friedman, M., Sosa, M.S., Sun, D., Dalla, E., Singh, D.K., Oktay, M.H., Aguirre-Ghiso, J.A., Condeelis, J.S., Entenberg, D., 2022. Primary tumor associated macrophages activate programs of invasion and dormancy in disseminating tumor cells. *Nature Communications* 2022 13:1 13, 1–19. <https://doi.org/10.1038/s41467-022-28076-3>
- Christmas, Brian J., Rafie, C.I., Hopkins, A.C., Scott, B.A., Ma, H.S., Cruz, K.A., Woolman, S., Armstrong, T.D., Connolly, R.M., Azad, N.A., Jaffee, E.M., Roussos Torres, E.T., 2018. Entinostat converts immune-resistant breast and pancreatic cancers into checkpoint-responsive tumors by reprogramming tumor-infiltrating MDSCs. *Cancer Immunol Res* 6, 1561–1577. <https://doi.org/10.1158/2326-6066.CIR-18-0070>
- Christmas, Brian J, Rafie, C.I., Hopkins, A.C., Scott, B.A., Ma, H.S., Cruz, K.A., Woolman, S., Armstrong, T.D., Connolly, R.M., Azad, N.A., Jaffee, E.M., Roussos Torres, E.T., 2018. Entinostat converts immune-resistant breast and pancreatic cancers into checkpoint-responsive tumors by reprogramming tumor-infiltrating MDSCs. *Cancer Immunol Res* canimm.0070.2018. <https://doi.org/10.1158/2326-6066.CIR-18-0070>

- Elaimy, A.L., Guru, S., Chang, C., Ou, J., Amante, J.J., Zhu, L.J., Goel, H.L., Mercurio, A.M., 2018. VEGF-neuropilin-2 signaling promotes stem-like traits in breast cancer cells by TAZ-mediated repression of the Rac GAP β 2-chimaerin. *Sci Signal* 11.
https://doi.org/10.1126/SCISIGNAL.AAO6897/SUPPL_FILE/AAO6897_SM.PDF
- Fares, J., Fares, M.Y., Khachfe, H.H., Salhab, H.A., Fares, Y., 2020. Molecular principles of metastasis: a hallmark of cancer revisited. *Signal Transduction and Targeted Therapy* 2020 5:1 5, 1–17. <https://doi.org/10.1038/s41392-020-0134-x>
- Fayard, B., Bianchi, F., Dey, J., Moreno, E., Djaffer, S., Hynes, N.E., Monard, D., 2009. The serine protease inhibitor protease nexin-1 controls mammary cancer metastasis through LRP-1-mediated MMP-9 expression. *Cancer Res* 69, 5690–5698.
<https://doi.org/10.1158/0008-5472.CAN-08-4573>
- Fry, E.A., Taneja, P., Inoue, K., 2017. Oncogenic and tumor-suppressive mouse models for breast cancer engaging HER2/neu. *Int J Cancer* 140, 495–503.
<https://doi.org/10.1002/IJC.30399>
- Gaude, E., Frezza, C., 2016. Tissue-specific and convergent metabolic transformation of cancer correlates with metastatic potential and patient survival. *Nat Commun* 7.
<https://doi.org/10.1038/NCOMMS13041>
- Gil Del Alcazar, C.R., Trinh, A., Alečković, M., Jimenez, E.R., Harper, N.W., Oliphant, M.U.J., Xie, S., Krop, E.D., Lulseged, B., Murphy, K.C., Keenan, T.E., Van Allen, E.M., Tolaney, S.M., Freeman, G.J., Dillon, D.A., Muthuswamy, S.K., Polyak, K., 2022. Insights into Immune Escape During Tumor Evolution and Response to Immunotherapy Using a Rat Model of Breast Cancer. *Cancer Immunol Res* 10, 680. <https://doi.org/10.1158/2326-6066.CIR-21-0804>
- Goswami, S., Philippar, U., Sun, D., Patsialou, A., Avraham, J., Wang, W., Di Modugno, F., Nistico, P., Gertler, F.B., Condeelis, J.S., 2009. Identification of invasion specific splice

- variants of the cytoskeletal protein Mena present in mammary tumor cells during invasion in vivo. *Clin Exp Metastasis* 26, 153. <https://doi.org/10.1007/S10585-008-9225-8>
- Green, J.E., Shibata, M.A., Yoshidome, K., Liu, M.L., Jorcyk, C., Anver, M.R., Wigginton, J., Wiltrout, R., Shibata, E., Kaczmarczyk, S., Wang, W., Liu, Z.Y., Calvo, A., Couldrey, C., 2000. The C3(1)/SV40 T-antigen transgenic mouse model of mammary cancer: ductal epithelial cell targeting with multistage progression to carcinoma. *Oncogene* 19, 1020–1027. <https://doi.org/10.1038/SJ.ONC.1203280>
- Gündüz, U.R., Gunaldi, M., Isiksacan, N., Gündüz, S., Okuturlar, Y., Kocoglu, H., 2016. A new marker for breast cancer diagnosis, human epididymis protein 4: A preliminary study. *Mol Clin Oncol* 5, 355. <https://doi.org/10.3892/MCO.2016.919>
- Guy, Chantale T, Cardiff, R.D., Muller`*, W.J., 1992. Induction of mammary tumors by expression of polyomavirus middle T oncogene: a transgenic mouse model for metastatic disease. *Mol Cell Biol* 12, 954. <https://doi.org/10.1128/MCB.12.3.954>
- Guy, C T, Webster, M.A., Schaller, M., Parsons, T.J., Cardiff, R.D., Muller, W.J., 1992. Expression of the neu protooncogene in the mammary epithelium of transgenic mice induces metastatic disease. *Proceedings of the National Academy of Sciences* 89, 10578–10582. <https://doi.org/10.1073/PNAS.89.22.10578>
- Helfman, D.M., Kim, E.J., Lukanidin, E., Grigorian, M., 2005. The metastasis associated protein S100A4: role in tumour progression and metastasis. *British Journal of Cancer* 2005 92:11 92, 1955–1958. <https://doi.org/10.1038/sj.bjc.6602613>
- Jaffee, E.M., Schutte, M., Gossett, J., Morsberger, L.A., Adler, A.J., Thomas, M., Greten, T.F., Hruban, R.H., Yeo, C.J., Griffin, C.A., 1998. Development and characterization of a cytokine-secreting pancreatic adenocarcinoma vaccine from primary tumors for use in clinical trials. *Cancer J Sci Am* 4, 194–203.
- Jansson, S., Aaltonen, K., Bendahl, P.O., Falck, A.K., Karlsson, M., Pietras, K., Rydén, L., 2018. The PDGF pathway in breast cancer is linked to tumour aggressiveness, triple-

negative subtype and early recurrence. *Breast Cancer Res Treat* 169, 231.

<https://doi.org/10.1007/S10549-018-4664-7>

Kalluri, R., Weinberg, R.A., 2009. The basics of epithelial-mesenchymal transition. *J Clin Invest* 119, 1420. <https://doi.org/10.1172/JCI39104>

Karagiannis, G.S., Goswami, S., Jones, J.G., Oktay, M.H., Condeelis, J.S., 2016. Signatures of breast cancer metastasis at a glance. *J Cell Sci* 129, 1751–1758.

<https://doi.org/10.1242/JCS.183129/-/DC2>

Karagiannis, G.S., Pastoriza, J.M., Wang, Y., Harney, A.S., Entenberg, D., Pignatelli, J., Sharma, V.P., Xue, E.A., Cheng, E., D'Alfonso, T.M., Jones, J.G., Anampa, J., Rohan, T.E., Sparano, J.A., Condeelis, J.S., Oktay, M.H., 2017. Neoadjuvant chemotherapy induces breast cancer metastasis through a TMEM-mediated mechanism. *Sci Transl Med* 9. <https://doi.org/10.1126/SCITRANSLMED.AAN0026>

Kim, I.S., Baek, S.H., 2010. Mouse models for breast cancer metastasis. *Biochem Biophys Res Commun* 394, 443–447. <https://doi.org/10.1016/J.BBRC.2010.03.070>

Kim, K., Skora, A.D., Li, Z., Liu, Q., Tam, A.J., Blosser, R.L., Diaz, L.A., Papadopoulos, N., Kinzler, K.W., Vogelstein, B., Zhou, S., 2014. Eradication of metastatic mouse cancers resistant to immune checkpoint blockade by suppression of myeloid-derived cells. *Proc Natl Acad Sci U S A* 111, 11774–11779. <https://doi.org/10.1073/PNAS.1410626111/-/DCSUPPLEMENTAL>

Kominsky, S.L., Argani, P., Korz, D., Evron, E., Raman, V., Garrett, E., Rein, A., Sauter, G., Kallioniemi, O.P., Sukumar, S., 2003. Loss of the tight junction protein claudin-7 correlates with histological grade in both ductal carcinoma in situ and invasive ductal carcinoma of the breast. *Oncogene* 22, 2021–2033. <https://doi.org/10.1038/SJ.ONC.1206199>

Kyung-A Hyun, Goo, K.B., Han, H., Sohn, J., Choi, W., Kim, S. II, Jung, H. II, Kim, Y.S., 2016. Epithelial-to-mesenchymal transition leads to loss of EpCAM and different physical

- properties in circulating tumor cells from metastatic breast cancer. *Oncotarget* 7, 24677.
<https://doi.org/10.18632/ONCOTARGET.8250>
- Le Bras, G.F., Taubenslag, K.J., Andl, C.D., 2012. The regulation of cell-cell adhesion during epithelial-mesenchymal transition, motility and tumor progression. *Cell Adh Migr* 6, 365.
<https://doi.org/10.4161/CAM.21326>
- Lin, S.C.J., Lee, K.F., Nikitin, A.Y., Hilsenbeck, S.G., Cardiff, R.D., Li, A., Kang, K.W., Frank, S.A., Lee, W.H., Lee, E.Y.H.P., 2004. Somatic mutation of p53 leads to estrogen receptor alpha-positive and -negative mouse mammary tumors with high frequency of metastasis. *Cancer Res* 64, 3525–3532. <https://doi.org/10.1158/0008-5472.CAN-03-3524>
- Liu, F., Gu, L.N., Shan, B.E., Geng, C.Z., Sang, M.X., 2016. Biomarkers for EMT and MET in breast cancer: An update. *Oncol Lett* 12, 4869. <https://doi.org/10.3892/OL.2016.5369>
- Ludyga, N., Englert, S., Pflieger, K., Rauser, S., Braselmann, H., Walch, A., Auer, G., Höfler, H., Aubele, M., 2013. The impact of Cysteine-Rich Intestinal Protein 1 (CRIP1) in human breast cancer. *Mol Cancer* 12, 28. <https://doi.org/10.1186/1476-4598-12-28>
- Ma, Y., Shepherd, J., Zhao, D., Bollu, L.R., Tahaney, W.M., Hill, J., Zhang, Y., Mazumdar, A., Brown, P.H., 2020. SOX9 Is Essential for Triple-Negative Breast Cancer Cell Survival and Metastasis. *Mol Cancer Res* 18, 1825–1838. <https://doi.org/10.1158/1541-7786.MCR-19-0311>
- Machiels, J.P., Reilly, R.T., Emens, L.A., Ercolini, A.M., Lei, R.Y., Weintraub, D., Okoye, F.I., Jaffee, E.M., 2001. Cyclophosphamide, doxorubicin, and paclitaxel enhance the antitumor immune response of granulocyte/macrophage-colony stimulating factor-secreting whole-cell vaccines in HER-2/neu tolerized mice. *Cancer Res* 61, 3689–97.
- Macleod, K.F., Jacks, T., 1999. INSIGHTS INTO CANCER FROM TRANSGENIC MOUSE MODELS. *J. Pathol* 187, 43–60. [https://doi.org/10.1002/\(SICI\)1096-9896\(199901\)187:1](https://doi.org/10.1002/(SICI)1096-9896(199901)187:1)

- Martin, T.A., Jiang, W.G., 2009. Loss of tight junction barrier function and its role in cancer metastasis. *Biochimica et Biophysica Acta (BBA) - Biomembranes* 1788, 872–891.
<https://doi.org/10.1016/J.BBAMEM.2008.11.005>
- Moraes, L.A., Ampomah, P.B., Lim, L.H.K., 2018. Annexin A1 in inflammation and breast cancer: a new axis in the tumor microenvironment. *Cell Adh Migr* 12, 417.
<https://doi.org/10.1080/19336918.2018.1486143>
- Orillion, A., Hashimoto, A., Damayanti, N., Shen, L., Adelaiye-Ogala, R., Arisa, S., Chintala, S., Ordentlich, P., Kao, C., Elzey, B., Gabrilovich, D., Pili, R., 2017. Entinostat Neutralizes Myeloid-Derived Suppressor Cells and Enhances the Antitumor Effect of PD-1 Inhibition in Murine Models of Lung and Renal Cell Carcinoma. *Clinical Cancer Research* 23, 5187–5201. <https://doi.org/10.1158/1078-0432.CCR-17-0741>
- Pal, A.K., Sharma, P., Zia, A., Siwan, D., Nandave, D., Nandave, M., Gautam, R.K., 2022. Metabolomics and EMT Markers of Breast Cancer: A Crosstalk and Future Perspective. *Pathophysiology* 2022, Vol. 29, Pages 200-222 29, 200–222.
<https://doi.org/10.3390/PATHOPHYSIOLOGY29020017>
- Park, M.K., Lee, C.H., Lee, H., 2018. Mouse models of breast cancer in preclinical research. *Lab Anim Res* 34, 160. <https://doi.org/10.5625/LAR.2018.34.4.160>
- Paulin, D., Lilienbaum, A., Kardjian, S., Agbulut, O., Li, Z., 2022. Vimentin: Regulation and pathogenesis. *Biochimie* 197, 96–112. <https://doi.org/10.1016/J.BIOCHI.2022.02.003>
- Philippar, U., Roussos, E.T., Oser, M., Yamaguchi, H., Kim, H. Do, Giampieri, S., Wang, Y., Goswami, S., Wyckoff, J.B., Lauffenburger, D.A., Sahai, E., Condeelis, J.S., Gertler, F.B., 2008. A Mena Invasion Isoform Potentiates EGF-Induced Carcinoma Cell Invasion and Metastasis. *Dev Cell* 15, 813. <https://doi.org/10.1016/J.DEVCEL.2008.09.003>
- Pinto, M.P., Dye, W.W., Jacobsen, B.M., Horwitz, K.B., 2014. Malignant stroma increases luminal breast cancer cell proliferation and angiogenesis through platelet-derived growth factor signaling. *BMC Cancer* 14. <https://doi.org/10.1186/1471-2407-14-735>

- Qiao, Y., Shiue, C.N., Zhu, J., Zhuang, T., Jonsson, P., Wright, A.P.H., Zhao, C., Dahlman-Wright, K., 2015. AP-1-mediated chromatin looping regulates ZEB2 transcription: new insights into TNF α -induced epithelial-mesenchymal transition in triple-negative breast cancer. *Oncotarget* 6, 7804–7814. <https://doi.org/10.18632/ONCOTARGET.3158>
- Rappa, G., Green, T.M., Karbanová, J., Corbeil, D., Lorico, A., 2015. Tetraspanin CD9 determines invasiveness and tumorigenicity of human breast cancer cells. *Oncotarget* 6, 7970. <https://doi.org/10.18632/ONCOTARGET.3419>
- Reilly, R T, Gottlieb, M.B., Ercolini, A.M., Machiels, J.P., Kane, C.E., Okoye, F.I., Muller, W.J., Dixon, K.H., Jaffee, E.M., 2000a. HER-2/neu is a tumor rejection target in tolerized HER-2/neu transgenic mice. *Cancer Res* 60, 3569–76.
- Reilly, R T, Gottlieb, M.B., Ercolini, A.M., Machiels, J.P., Kane, C.E., Okoye, F.I., Muller, W.J., Dixon, K.H., Jaffee, E.M., 2000b. HER-2/neu is a tumor rejection target in tolerized HER-2/neu transgenic mice. *Cancer Res* 60, 3569–76.
- Reilly, R Todd, Gottlieb, M.B.C., Ercolini, A.M., Machiels, J.-P.H., Kane, C.E., Okoye, F.I., Muller, W.J., Dixon, K.H., Jaffee, E.M., 2000. HER-2/neu Is a Tumor Rejection Target in Tolerized HER-2/neu Transgenic Mice¹. *Cancer Res* 60, 3569–3576.
- Riggio, A.I., Varley, K.E., Welm, A.L., 2020. The lingering mysteries of metastatic recurrence in breast cancer. *British Journal of Cancer* 2020 124:1 124, 13–26. <https://doi.org/10.1038/s41416-020-01161-4>
- Robinson, B.D., Sica, G.L., Liu, Y.F., Rohan, T.E., Gertler, F.B., Condeelis, J.S., Jones, J.G., 2009. Tumor Microenvironment of Metastasis in Human Breast Carcinoma: A Potential Prognostic Marker Linked to Hematogenous Dissemination. *Clin Cancer Res* 15, 2433. <https://doi.org/10.1158/1078-0432.CCR-08-2179>
- Roussos, E.T., Balsamo, M., Alford, S.K., Wyckoff, J.B., Gligorijevic, B., Wang, Y., Pozzuto, M., Stobezki, R., Goswami, S., Segall, J.E., Lauffenburger, D.A., Bresnick, A.R., Gertler, F.B., Condeelis, J.S., 2011a. Mena invasive (Mena^{INV}) promotes multicellular streaming motility

and transendothelial migration in a mouse model of breast cancer. *J Cell Sci* 124, 2120.

<https://doi.org/10.1242/JCS.086231>

Roussos, E.T., Goswami, S., Balsamo, M., Wang, Y., Stobezki, R., Adler, E., Robinson, B.D., Jones, J.G., Gertler, F.B., Condeelis, J.S., Oktay, M.H., 2011b. Mena invasive (MenaINV) and Mena11a isoforms play distinct roles in breast cancer cell cohesion and association with TMEM. *Clin Exp Metastasis* 28, 515–527. <https://doi.org/10.1007/S10585-011-9388-6/FIGURES/7>

Seaman, S., Zhu, Z., Saha, S., Zhang, X.M., Yang, M.Y., Hilton, M.B., Morris, K., Szot, C., Morris, H., Swing, D.A., Tessarollo, L., Smith, S.W., Degrado, S., Borkin, D., Jain, N., Scheiermann, J., Feng, Y., Wang, Y., Li, J., Welsch, D., DeCrescenzo, G., Chaudhary, A., Zudaire, E., Klarmann, K.D., Keller, J.R., Dimitrov, D.S., St. Croix, B., 2017. Eradication of Tumors through Simultaneous Ablation of CD276/B7-H3 Positive Tumor Cells and Tumor Vasculature. *Cancer Cell* 31, 501. <https://doi.org/10.1016/J.CCELL.2017.03.005>

Sharma, V.P., Tang, B., Wang, Y., Duran, C.L., Karagiannis, G.S., Xue, E.A., Entenberg, D., Borriello, L., Coste, A., Eddy, R.J., Kim, G., Ye, X., Jones, J.G., Grunblatt, E., Agi, N., Roy, S., Bandyopadhyaya, G., Adler, E., Surve, C.R., Esposito, D., Goswami, S., Segall, J.E., Guo, W., Condeelis, J.S., Wakefield, L.M., Oktay, M.H., 2021. Live tumor imaging shows macrophage induction and TMEM-mediated enrichment of cancer stem cells during metastatic dissemination. *Nature Communications* 2021 12:1 12, 1–24.

<https://doi.org/10.1038/s41467-021-27308-2>

Sidiropoulos, D.N., Rafie, C.I., Jang, J.K., Castanon, S., Baugh, A.G., Gonzalez, E., Christmas, B.J., Narumi, V.H., Davis-Marcisak, E.F., Sharma, G., Bigelow, E., Vaghasia, A., Gupta, A., Skaist, A., Considine, M., Wheelan, S.J., Ganesan, S.K., Yu, M., Yegnasubramanian, S., Stearns, V., Connolly, R.M., Gaykalova, D.A., Kagohara, L.T., Jaffee, E.M., Fertig, E.J., Roussos Torres, E.T., 2022. Entinostat decreases immune suppression to promote anti-

- tumor responses in a HER2+ breast tumor microenvironment. *Cancer Immunol Res* canimm.0170.2021. <https://doi.org/10.1158/2326-6066.CIR-21-0170>
- Siegel, P.M., Shu, W., Cardiff, R.D., Muller, W.J., Massagué, J., 2003. Transforming growth factor β signaling impairs Neu-induced mammary tumorigenesis while promoting pulmonary metastasis. *Proc Natl Acad Sci U S A* 100, 8430. <https://doi.org/10.1073/PNAS.0932636100>
- Song, H., Shahverdi, K., Huso, D.L., Wang, Y., Fox, J.J., Hobbs, R.F., Gimi, B., Gabrielson, K.L., Pomper, M.G., Tsui, B.M., Bhujwala, Z., Reilly, R.T., Sgouros, G., 2008. An Immunotolerant HER-2/neu Transgenic Mouse Model of Metastatic Breast Cancer. *Clin Cancer Res* 14, 6116. <https://doi.org/10.1158/1078-0432.CCR-07-4672>
- Sundqvist, A., Morikawa, M., Ren, J., Vasilaki, E., Kawasaki, N., Kobayashi, M., Koinuma, D., Aburatani, H., Miyazono, K., Heldin, C.H., Van Dam, H., Dijke, P. Ten, 2018. JUNB governs a feed-forward network of TGF β signaling that aggravates breast cancer invasion. *Nucleic Acids Res* 46, 1180. <https://doi.org/10.1093/NAR/GKX1190>
- Sung, H., Ferlay, J., Siegel, R.L., Laversanne, M., Soerjomataram, I., Jemal, A., Bray, F., 2021. Global Cancer Statistics 2020: GLOBOCAN Estimates of Incidence and Mortality Worldwide for 36 Cancers in 185 Countries. *CA Cancer J Clin* 71, 209–249. <https://doi.org/10.3322/CAAC.21660>
- Vogel, C.L., Cobleigh, M.A., Tripathy, D., Gutheil, J.C., Harris, L.N., Fehrenbacher, L., Slamon, D.J., Murphy, M., Novotny, W.F., Burchmore, M., Shak, S., Stewart, S.J., Press, M., 2002. Efficacy and safety of trastuzumab as a single agent in first-line treatment of HER2-overexpressing metastatic breast cancer. *Journal of Clinical Oncology* 20, 719–726. <https://doi.org/10.1200/JCO.20.3.719>
- Xing, P., Liao, Z., Ren, Z., Zhao, J., Song, F., Wang, G., Chen, K., Yang, J., 2016. Roles of low-density lipoprotein receptor-related protein 1 in tumors. *Chin J Cancer* 35, 6. <https://doi.org/10.1186/S40880-015-0064-0>

- Yang, C., Yu, H., Chen, R., Tao, K., Lei, J., Peng, M., Li, X., Liu, M., Liu, S., 2019. CXCL1 stimulates migration and invasion in ER-negative breast cancer cells via activation of the ERK/MMP2/9 signaling axis. *Int J Oncol* 55, 684–696.
<https://doi.org/10.3892/IJO.2019.4840>
- Yang, J., Bielenberg, D.R., Rodig, S.J., Doiron, R., Clifton, M.C., Kung, A.L., Strong, R.K., Zurakowski, D., Moses, M.A., 2009. Lipocalin 2 promotes breast cancer progression. *Proc Natl Acad Sci U S A* 106, 3913–3918.
https://doi.org/10.1073/PNAS.0810617106/SUPPL_FILE/0810617106SI.PDF
- Yasuoka, H., Kodama, R., Tsujimoto, M., Yoshidome, K., Akamatsu, H., Nakahara, M., Inagaki, M., Sanke, T., Nakamura, Y., 2009. Neuropilin-2 expression in breast cancer: correlation with lymph node metastasis, poor prognosis, and regulation of CXCR4 expression. *BMC Cancer* 9, 220. <https://doi.org/10.1186/1471-2407-9-220/FIGURES/4>
- Yeo, S.K., Zhu, X., Okamoto, T., Hao, M., Wang, C., Lu, P., Lu, L.J., Guan, J.L., 2020. Single-cell RNA-sequencing reveals distinct patterns of cell state heterogeneity in mouse models of breast cancer. *Elife* 9, 1–24. <https://doi.org/10.7554/ELIFE.58810>
- Yu, Y., Wang, W., Lu, W., Chen, W., Shang, A., 2021. Inhibin β -A (INHBA) induces epithelial–mesenchymal transition and accelerates the motility of breast cancer cells by activating the TGF- β signaling pathway. *Bioengineered* 12, 4681.
<https://doi.org/10.1080/21655979.2021.1957754>
- Zhang, H., Fu, L., 2021. The role of ALDH2 in tumorigenesis and tumor progression: Targeting ALDH2 as a potential cancer treatment. *Acta Pharm Sin B* 11, 1400.
<https://doi.org/10.1016/J.APSB.2021.02.008>

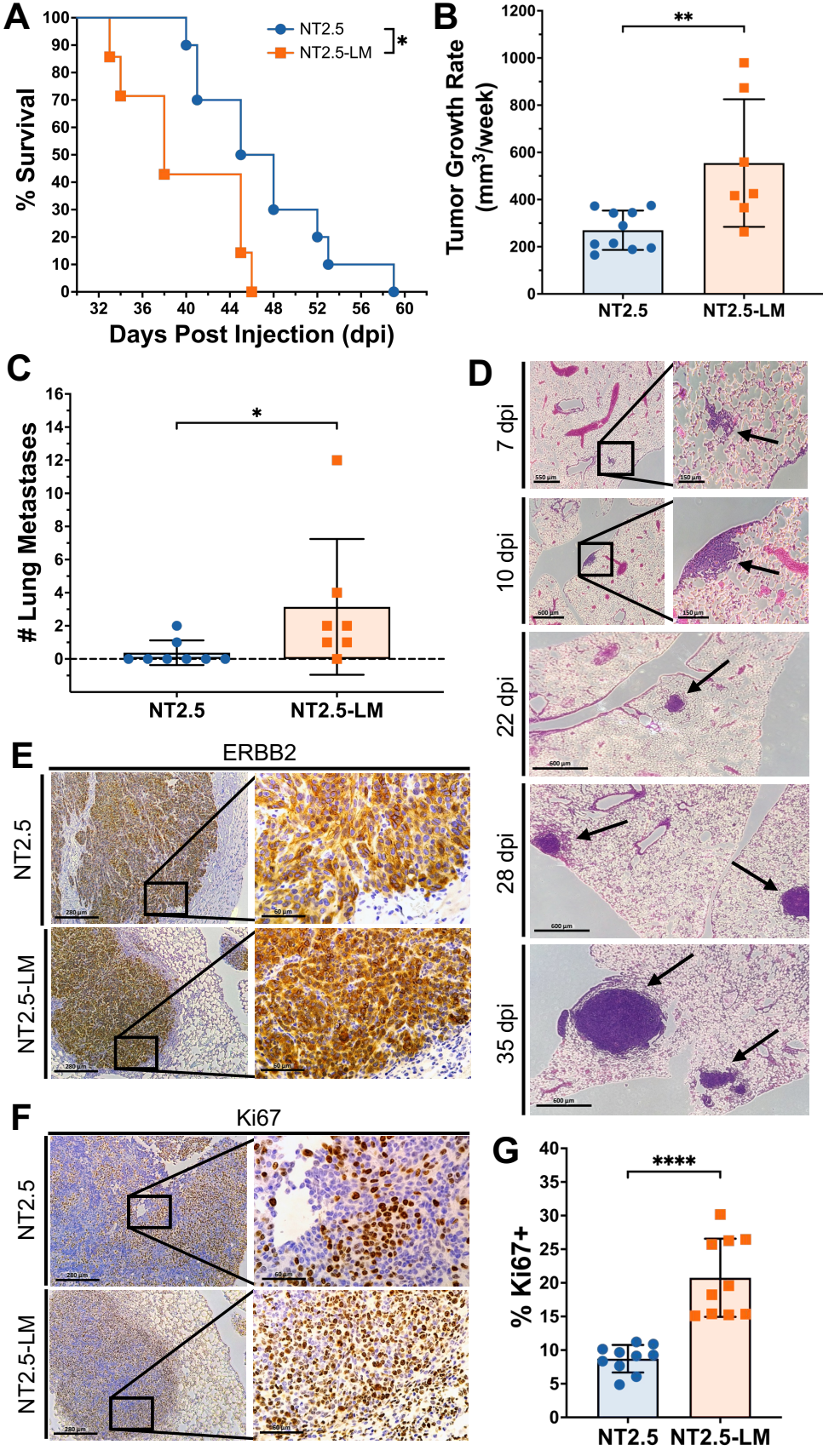


Figure 1

Figure 1: NT2.5-LM leads to decreased survival, larger mammary tumors, and increased lung metastasis. (A) 1×10^5 NT2.5 or NT2.5-LM cells were injected into the mammary fat pad of NeuN mice (NT2.5, n=10; NT2.5-LM, n=7). After surgical resection of NT2.5-LM tumor-bearing mice at 12 days post-injection (dpi), mice were allowed to reach human survival endpoint with tumor volume exceeding 1.5 cm^3 . (B) Mammary tumor sizes of mice in (A) were measured at least 3x a week by calipers, averaged, and used to calculate differences in average weekly tumor growth rate. (C) At survival endpoint of mice in (A), the number of surface metastases was counted by visual inspection. (D) H&E staining of lungs in NT2.5-LM tumor-bearing mice collected at 7, 10, 22, 28, and 35 days post-injection (dpi). Black arrows point to lung metastases. Scale bars as shown. (E) Immunohistochemistry (IHC) staining of Erbb2 and (F) Ki67 in NT2.5 mammary tumors (top) and NT2.5-LM lung metastases (bottom) collected at 35 days post-injection. Scale bars as shown. (G) Percentage of Ki67+ cells from 10 regions of interest (ROIs) were counted from Ki67 IHC staining in (F). Statistics used: Mantel-Cox Log-rank test for (A), Mann-Whitney U-test for (B-D), Welch's T-test for (G), *p < 0.05, **p < 0.01, ****p < 0.0001.

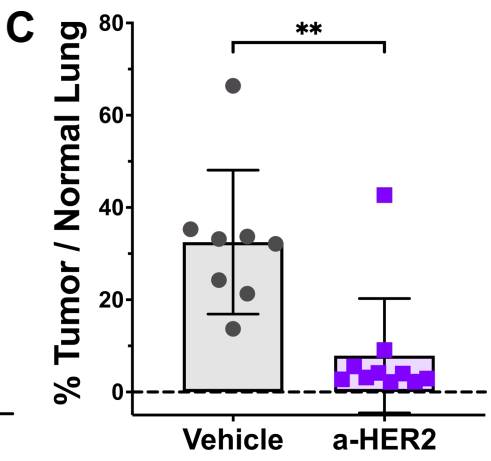
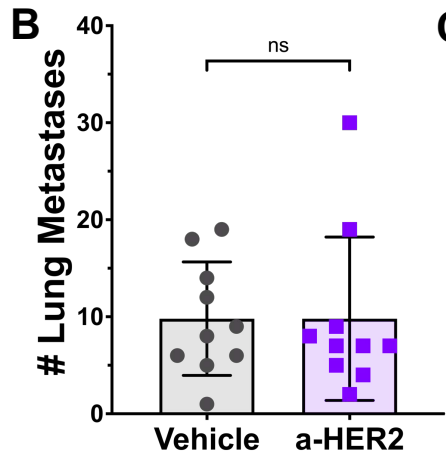
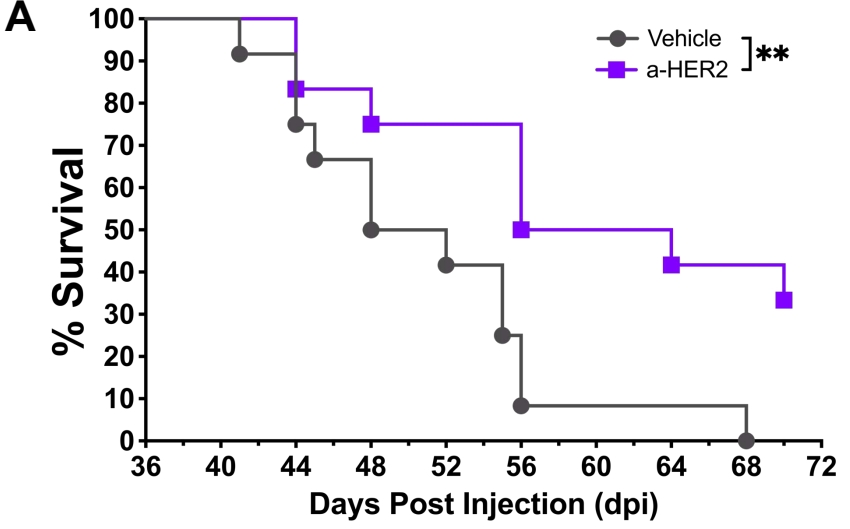
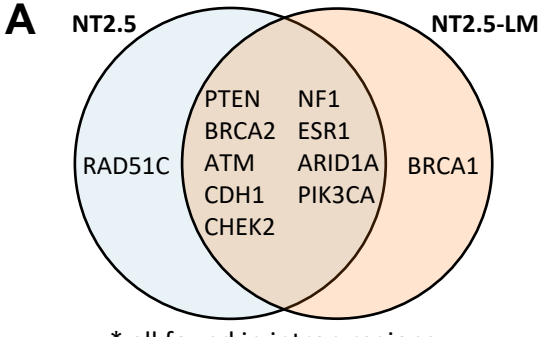


Figure 2

Figure 2: NT2.5-LM responds to HER2-directed therapy. (A) 1×10^5 NT2.5-LM cells were injected into the mammary fat pad of NeuN mice. After surgical resection of NT2.5-LM tumor-bearing mice at 12 days post-injection (dpi), treatment with vehicle or anti-HER2 monoclonal antibody (100 $\mu\text{g}/\text{mouse}$, 1x/week, intraperitoneal injection) began at 23 dpi (n=12 per treatment group) and continued until survival endpoint at 70 dpi. **(B)** 1×10^5 NT2.5-LM cells were injected into the mammary fat pad of NeuN mice, tumors were surgically resected at 12 dpi, and anti-HER2 treatment (100 $\mu\text{g}/\text{mouse}$, 1x/week, intraperitoneal injection) began at 23 dpi (n=10 per treatment group). Lungs were collected at 38 dpi. Three different levels were taken from formalin-fixed and paraffin-embedded lungs sectioned 100 μm apart. Slides were H&E stained, scanned, and analyzed using HALO to obtain summed lung metastasis counts and **(C)** percent tumor area over normal lung tissue. Two mice in the vehicle group were removed due to inconsistencies between HALO results and physical examination of H&E slides. Statistics used: Mantel-Cox Log-rank test for (A), Mann-Whitney U-test for (B-C), ns = not-significant, **p < 0.01.

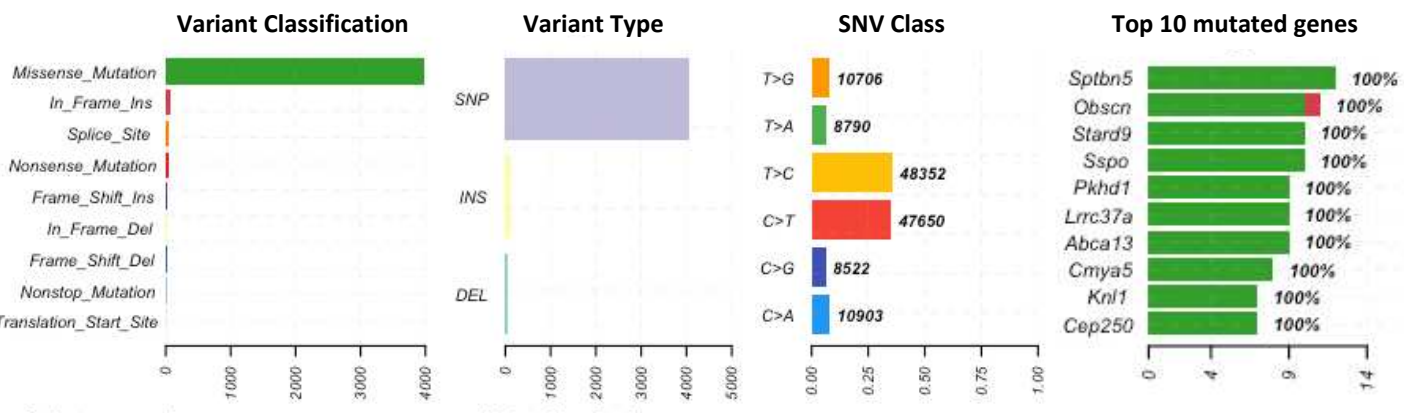


* all found in intron regions

B

Nucleotide change	Amino acid – change (Y/N)	Mutation site	Mutation type	Model
c.1937G>A	p.Glu58 - N	Exon 15	Silent	NT2.5-LM
c.2081A>C	p.Ser634 - N	Exon 16	Silent	NT2.5 NT2.5-LM
c.2336A>G	p.Thr719 - N	Exon 18	Silent	NT2.5 NT2.5-LM
c.2522A>G	p.Pro781 - N	Exon 20	Silent	NT2.5-LM

C NT2.5



D NT2.5-LM

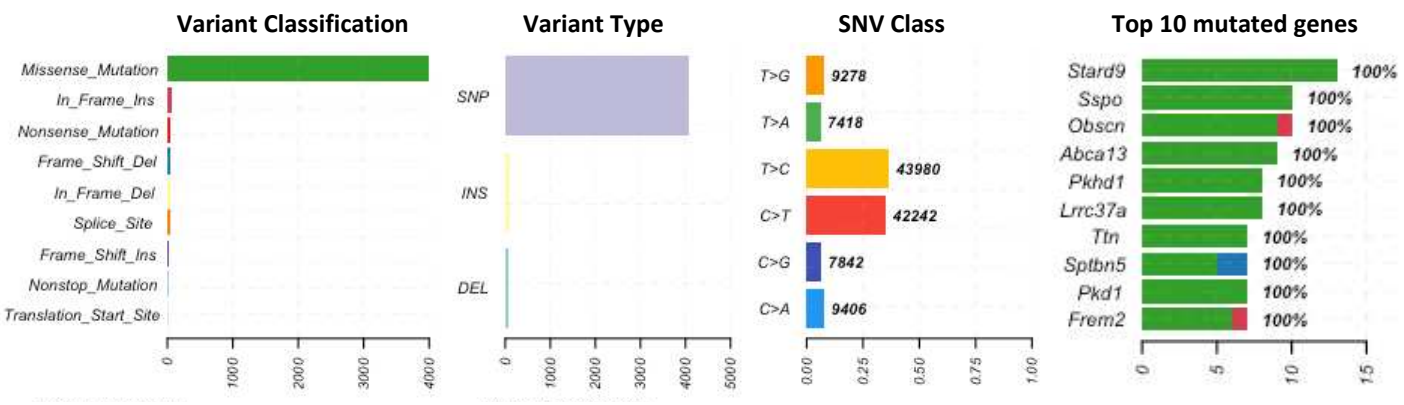


Figure 3

Figure 3: NT2.5-LM does not exhibit altered mutational landscape compared to parental NT2.5. (A) Alignment of NT2.5 and NT2.5-LM whole exome sequencing reads to the mm10 genome reveal cell line-specific and –overlapping mutations common in breast cancer. Note: all found were in intronic regions. **(B)** ErbB2 transcript sequence with identified mutation sites in NT2.5 and NT2.5-LM. All mutations were identified to be silent mutations. Nucleotide numbering is based on DNA reference sequence NM_001003817.1. Note that the version number of this reference sequence may be frequently updated. **(C)** Distributions of mutation classifications, variant types, single nucleotide variant (SNV) classes, and top 10 mutated genes for NT2.5 and **(D)** NT2.5-LM are shown.

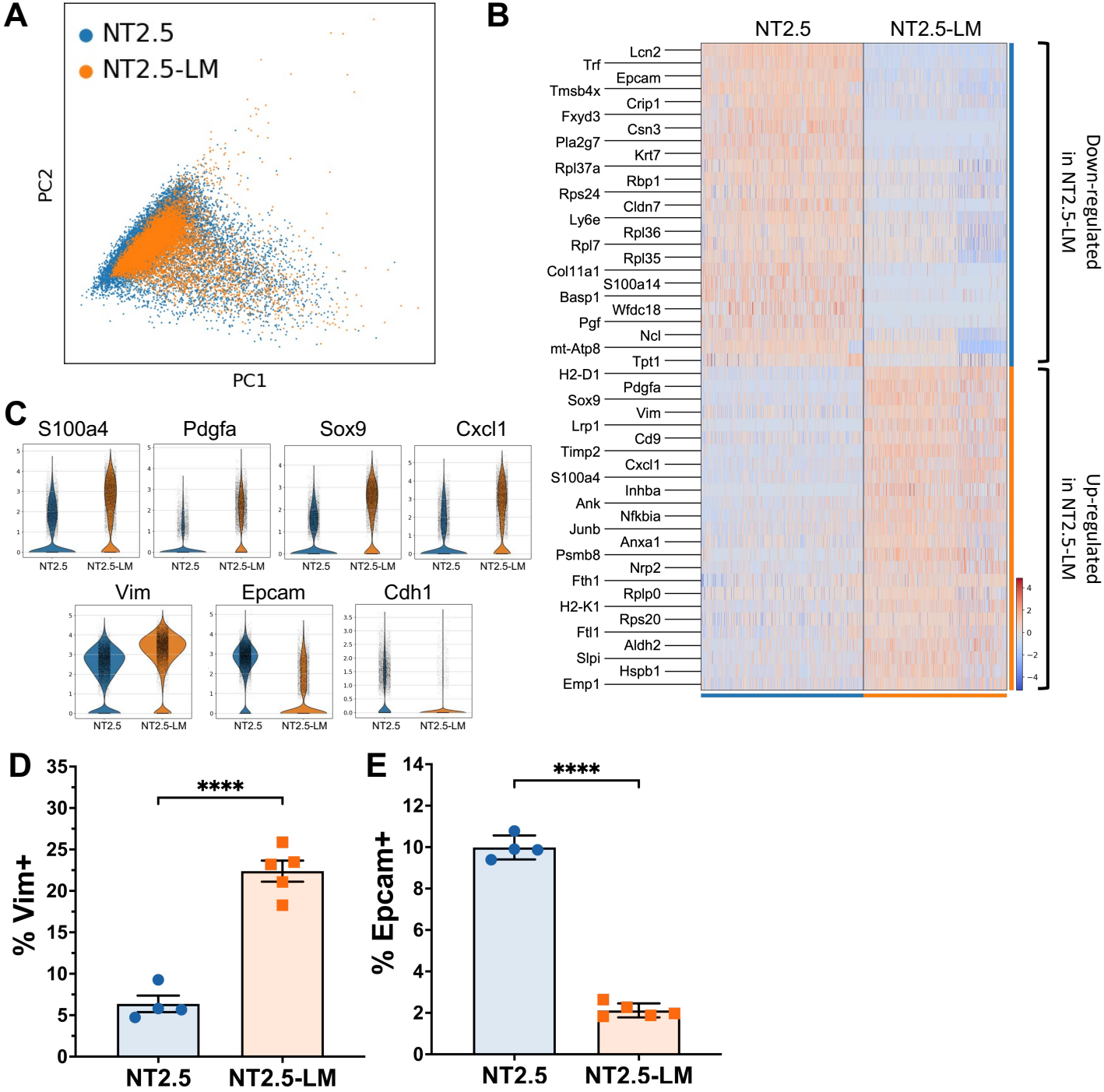


Figure 4

Figure 4: NT2.5-LM exhibits altered signaling indicative of increased EMT. (A) Four NT2.5 and four NT2.5-LM mammary tumors were collected from NeuN mice, dissociated to single cell suspensions, and sent for unsorted single-cell RNA sequencing. Cancer cell clusters were annotated as *Lcn+*, *Wfd2c+*, *Cd24a+*, *Cd276+*, *Col9a1+*, *Erb2+*, and subsetted out for PCA visualization. **(B)** Top 25 significantly up- and down-regulated genes in NT2.5-LM. **(C)** Violin plots of key metastasis-related genes identified in (B). **(D)** Flow cytometry staining of epithelial-to-mesenchymal transition (EMT) related genes identified in (C) in NT2.5 and NT2.5-LM cell lines for Vimentin and **(E)** Epcam. Statistics used: Unpaired T-test for (D-E), ****p < 0.0001.

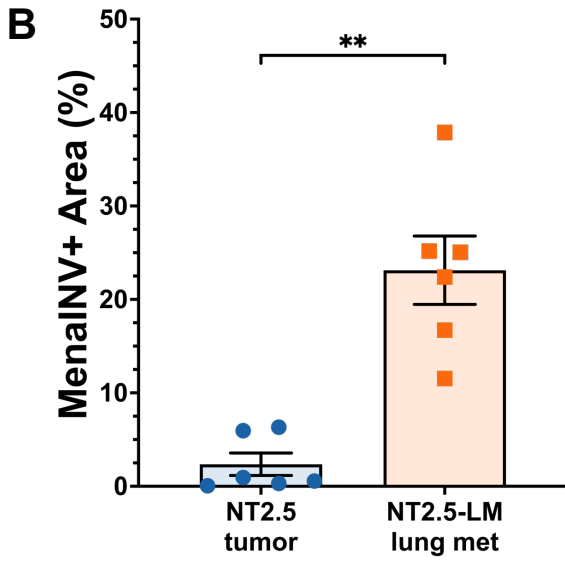
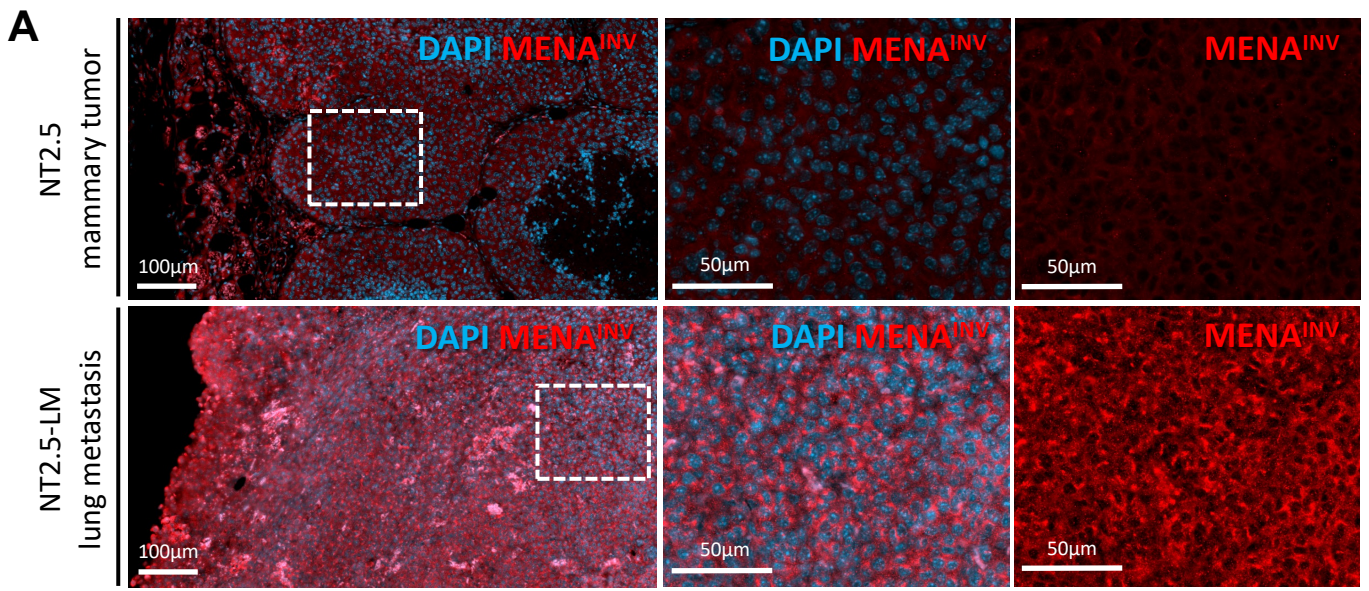


Figure 5

Figure 5: NT2.5-LM expresses increased levels of Mena^{INV} – a marker of metastatic potential. (A) Representative immunofluorescence images of Mena^{INV} (red) and DAPI (blue) staining in NT2.5 mammary tumor (top), and NT2.5-LM lung metastases (bottom) collected 34-41 days post-injection (dpi). Middle column and right column panels correspond to dotted square in left column panels. Scale bars as shown.

(B) Quantification of Mena^{INV} staining from NT2.5 mammary tumor (n=6) and NT2.5-LM lung metastases (n=6) by averaging signal intensity from up to 10 regions of interest (ROIs) in each sample. Statistics used: Mann-Whitney U-test for (B), **p < 0.01.